Spin-orbit-coupling-induced half-skyrmion excitations in rotating and rapidly quenched spin-1 Bose-Einstein condensates

Chao-Fei Liu[1,2] and W. M. Liu[2]

[1]*School of Science, Jiangxi University of Science and Technology, Ganzhou 341000, China*
[2]*Beijing National Laboratory for Condensed Matter Physics, Institute of Physics, Chinese Academy of Sciences, Beijing 100190, China*

We investigate the half-skyrmion excitations induced by spin-orbit coupling in the rotating and rapidly quenched spin-1 Bose-Einstein condensates. We give three expressions of the corresponding spin vectors to describe the half-skyrmion. Our results show that the half-skyrmion excitation depends on the combination of spin-orbit coupling and rotation, and it originates from a dipole structure of spin which is always embedded in three vortices constructed by each condensate component respectively. When both the strength of spin-orbit coupling and the rotation frequency are larger than some critical values, the half-skyrmions encircle the center with one or several circles to form a radial lattice, which occurs even in the strong ferromagnetic/antiferromagnetic condensates. We can use both the spin-orbit coupling and the rotation to adjust the radial lattice. The realization and the detection of the half-skyrmions are compatible with current experimental technology.

I. INTRODUCTION

Spin-orbit coupling (SOC) describes the interaction of the spin of a particle with its motion. The particular form of SOC can be of either Bychkov-Rashba [1] or Dresselhaus [2] type. SOC in an electronic system [3] is able to serve as a spin filter or a Stern-Gerlach apparatus. And it is crucial for the spin-Hall effect [4,5] and topological insulators [6–9]. Recently, spin-orbit-coupled Bose-Einstein condensate (BEC) has been realized experimentally at the NIST [10]. Unlike the previous experiment, their work has factually explored the boson system in the non-Abelian gauge field [11–18]. This has opened up a new avenue in cold atom physics and has attracted much attention.

Motivated by the experiment at the NIST [10], several recent investigations about bosons with SOC have presented some nontrivial structures such as the stripe phase [19–22] and the half-quantum vortex state [21–24]. Specially, the combination effect of SOC and rotation on pseudo-spin-$\frac{1}{2}$ BEC has been shown to be able to generate various vortex structures [25,26]. These impressive results enrich the phase diagram of the BEC system. However, as a new effect on spinor BEC, it is not clear whether SOC can produce previously unknown types of topological excitations such as new skyrmions. The study of this topic, on the one hand, can fertilize the quantum phases in the BEC system and, on the other hand, can provide a systematic description of the BEC system with various adjusting parameters related to SOC, rotation, and quench, etc. This provides a realizable experimental platform for various quantum phenomena.

In this paper, we explore how SOC induces the half-skyrmion excitation whose topological charge is $|Q| = 0.5$ in the rotating spin-1 BEC. In real experiments, the zero temperature cannot be fully achieved. So the ultracold Bose gases are only partially condensed, with the noncondensed thermal cloud providing a source of dissipation and leading to damping excitations. Meanwhile, evaporative cooling is a critical operation to obtain the condensate. Thus, it is

necessary to refer to the finite-temperature effect and a quenching process. Furthermore, the rotation is a good tool to examine the excitations in spinor BECs [27–29]. Here, we just consider the quenching and the rotation process on the spin-1 BEC with SOC. We find that the half-skyrmion excitation (nonmeron-antimeron pair) is related to a three-vortex structure caused by SOC. We give a representation of the half-skyrmion. The phase diagram of this system is plotted in the plane of rotation frequency and SOC strength. We find that the generation of the half-skyrmion excitation must depend on the combination of SOC and rotation. Without SOC, the skyrmion excitation with topological charge $|Q| = 1$ occurs in the rotating ferromagnetic BECs. When both the strength of SOC and the rotation frequency are larger than some critical values, the half-skyrmions encircle the center of the system with one or several circles to form a radial lattice. These phenomena can occur even in the strong ferromagnetic/antiferromagnetic BECs. We can adjust the half-skyrmion lattice by changing the strength of SOC as well as rotation.

The paper is organized as follows: In Sec. II we introduce the stochastic projected Gross-Pitaevskii equations and some initial condition for our simulations. Section III is our main results and some explanations. In Sec. III A we use the rotating spin-1 BECs with SOC to obtain a single half-skyrmion. We not only illuminate the essence of the half-skyrmion excitation but also indicate the expressions to describe it. In Sec. III B the half-skyrmion lattice is studied. We further illuminate the relationship between the vortex structure and the half-skyrmion. We also show that the density distribution and the spin texture are dynamically stable when the system reaches the equilibrium state. In Sec. III C the effect of the rotation frequency is discussed. Then, we present the phase diagrams for generating the half-skyrmions and others. In Sec. III D we show that the half-skyrmion can occur in the strong ferromagnetic BECs and the strong antiferromagnetic BECs with both SOC and rotation. A summary of the paper is presented in Sec. IV.

II. MODEL AND EQUATION

Considered a quenching process in finite-temperature BECs, the dynamics of a spin-1 BEC can be described by the stochastic projected Gross-Pitaevskii equation (SPGPE) [30–32]. In the SPGPEs, the system is divided into the coherent region and the incoherent region. The coherent region consists of all states whose energies are below E_R and the incoherent region contains the remaining high energy modes. This division is made by the projection operation $\mathcal{P}$. The equations of motion are written in the form [30–32]

$$d\Psi_j = \mathcal{P}\left\{-\frac{i}{\hbar}\widehat{H}_j\Psi_j dt + \frac{\gamma_j}{k_B T}(\mu - \widehat{H}_j)\Psi_j dt + dW_j\right\},$$
(1)

where T is the final temperature, k_B is the Boltzmann constant, μ is the chemical potential, γ_j is the growth rate for the jth component, and dW_j is the complex Gaussian noise, which satisfies the fluctuation-dissipation relation $\langle dW_i^*(\mathbf{x},t)dW_j(\mathbf{x}',t)\rangle = 2\gamma_j\delta_{ij}\delta_C(\mathbf{x} - \mathbf{x}')dt$, where δ_C is the Dirac δ function for the condensate band field. The projection operator $\mathcal{P}$ is used to restrict the dynamics of the spinor BEC in the coherent region. Meanwhile, $\Psi_j(j = 0, \pm 1)$ denotes the macroscopic wave function of the atoms condensed in the spin state $|F = 1, m_F = j\rangle$, and

$$\widehat{H}_j\Psi_j = \left[-\frac{\hbar^2\nabla^2}{2m} + V(r) + g_n|\mathbf{\Psi}|^2\right]\Psi_j$$
$$+ g_s\sum_{\alpha=x,y,z}\sum_{n,k,l=0\pm 1}(\widehat{F}_\alpha)_{jn}(\widehat{F}_\alpha)_{kl}\Psi_n\Psi_k^*\Psi_l$$
$$- \Omega\widehat{L}_z\Psi_j + \sum_{\alpha=x,y}\sum_{n=0\pm 1}\kappa_\alpha(\widehat{F}_\alpha)_{jn}p_\alpha\Psi_n, \quad (2)$$

with the coupling constants $g_n = \frac{4\pi\hbar^2(2a_2+a_0)}{3m}$ and $g_s = \frac{4\pi\hbar^2(a_2-a_0)}{3m}$ and the trap potential $V(r) = m\omega^2(x^2 + y^2)/2$. $\widehat{F}_{\alpha=x,y,z}$ are the spin-1 matrices, Ω is the rotation frequency, $\widehat{L}_z [\widehat{L}_z = -i\hbar(x\partial_y - y\partial_x)]$ is the z component of the orbital angular momentum, $p (p_\alpha = -i\hbar\frac{\partial}{\partial\alpha}, \alpha = x,y)$ is the momentum operator, and κ_α denotes the strength of the SOC which carries the unit of velocity.

In numerical simulations, the initial state of each Ψ_j is generated by sampling the grand canonical ensemble for a free ideal Bose gas with the temperature T_0 and the chemical potential $\mu_{j,0}$. Meanwhile, the condensate band must lie below the energy cutoff $E_R > E_k = \frac{\hbar^2|k|^2}{2m}$. Note that $k = 2\pi(n_x, n_y)/L$, where n_x and n_y are integers and L is the size of the computation domain. To simulate the quenching process, the final temperature and the chemical potential of the noncondensate band are altered to the new values $T < T_0$ and $\mu > \mu_{j,0}(j = 0, \pm 1)$. Furthermore, we use the oscillator unit in the numerical computations. The length, time, energy, and strength of SOC are scaled in units of $\sqrt{\frac{\hbar}{m\omega}}$, ω^{-1}, $\hbar\omega$, and $\sqrt{\hbar\omega/m}$, respectively. In all the simulations, the trapped frequency is $\omega = 200 \times 2\pi$, the total number of the modes are n_x and $n_y = 300$, the energy cutoff is chosen at n_{xc}

and $n_{yc} = 150$, the initial temperature T_0 is 52 nK, the final temperature T is 10 nK, and we use $\frac{\gamma_j}{k_B T} = 0.03$.

III. RESULTS AND EXPLANATIONS

A. A half-skyrmion in spinor BEC with spin-orbit coupling

We first present a way to obtain a single half-skyrmion (nonmeron-antimeron pair) in the rotating spin-1 BEC with SOC. We begin with the spinor BEC of ^{87}Rb [33], which is ferromagnetic (FM) $(g_s < 0)$. We set our model with $\mu_{j,0}(j = 0, \pm 1) = 1.1\hbar\omega, \mu = 8\hbar\omega, \kappa_x = 0.2, \kappa_y = 1$, and the rotating frequency $\Omega = 0.5\omega$. Figure 1(a) displays the densities and
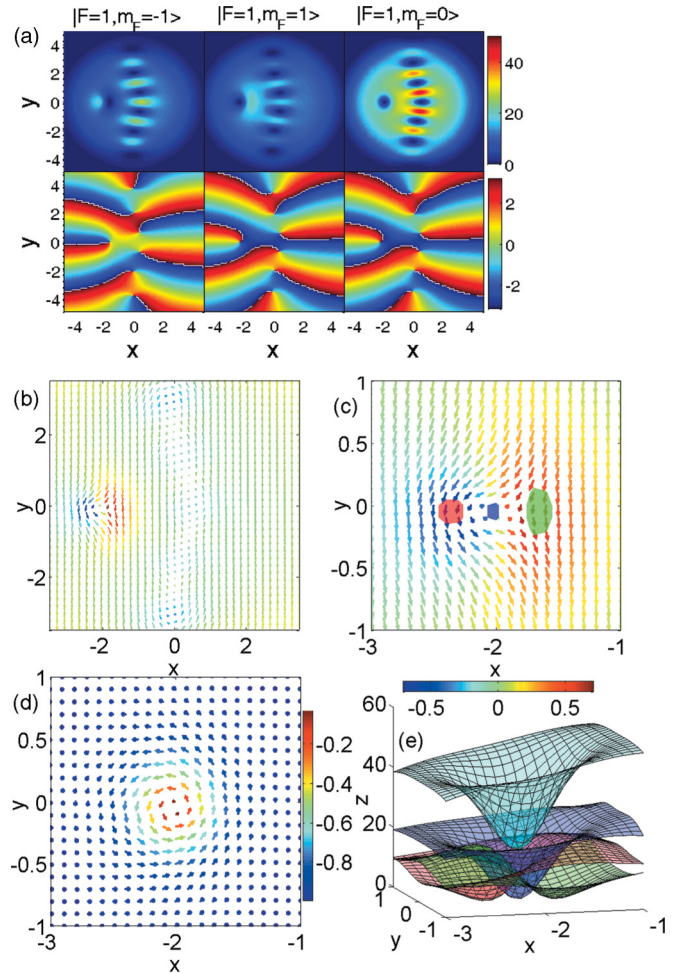

FIG. 1. (Color online) (a) The densities and phases for the spinor BEC of ^{87}Rb when the system reaches the equilibrium state, where $\kappa_x = 0.2$, $\kappa_y = 1$, $\mu = 8\hbar\omega$, and $\Omega = 0.5\omega$. The atom numbers are $N_{-1} \approx 510$, $N_1 \approx 540$, and $N_0 \approx 1050$. (b) Spin texture of the spinor BEC. The color of each arrow indicates the magnitude of S_z. (c) The position of vortices and the spin texture. The green, blue, and red spots are the center of vortices formed by the $m_F = -1$, $m_F = 0$, and $m_F = +1$ components, respectively. (d) Spin texture under the transformation: $(S_x', S_y', S_z') = (S_x, S_z, S_y)$. (e) A scheme of the three-vortex structure. The green, blue, and red surfaces denote the densities of the $m_F = -1$, $m_F = 0$, and $m_F = +1$ components, respectively. The cyan is the total density of the BECs. The units of length and strength of SOC are $\sqrt{\frac{\hbar}{m\omega}}$ and $\sqrt{\hbar\omega/m}$, respectively.
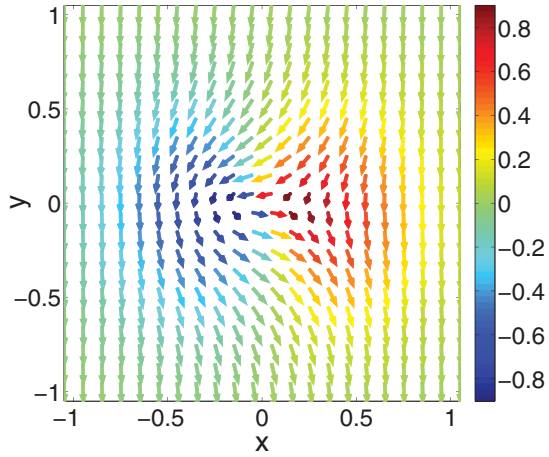
FIG. 2. (Color online) (a) Spin texture with Eqs. (4), where $\lambda = 0.5$. The color of each arrow indicates the magnitude of s_{0z}.

phases obtained under the equilibrium state. Obviously, there are several vortices in each component.

The spin texture [34–37] is defined by

$$\mathbf{S}_\alpha = \sum_{m,n=0,\pm 1} \Psi_m^* (\widehat{F}_\alpha)_{m,n} \Psi_n / |\mathbf{\Psi}|^2 (\alpha = x, y, z). \quad (3)$$

Figure 1(b) shows the corresponding spin texture according to Eq. (3). The direction of arrow changes suddenly and the arrows form a small half circle located near the position $(-2, 0)$. Additionally, the orientations of the arrows suffer a $180°$ reversal along the x axis. For clarification, Figure 1(c) plots an enlarged picture of the special structure. Note that, for illuminating the relationship between the structure and the vortices, we have added the position of the vortex in the three components with the color spots. We find the structure can be represented by the form

$$s_{0x} = -\frac{y}{\sqrt{x^2 + y^2}} \exp[-\lambda(x^2 + y^2)],$$

$$s_{0z} = \frac{x}{\sqrt{x^2 + y^2}} \exp[-\lambda(x^2 + y^2)], \quad (4)$$

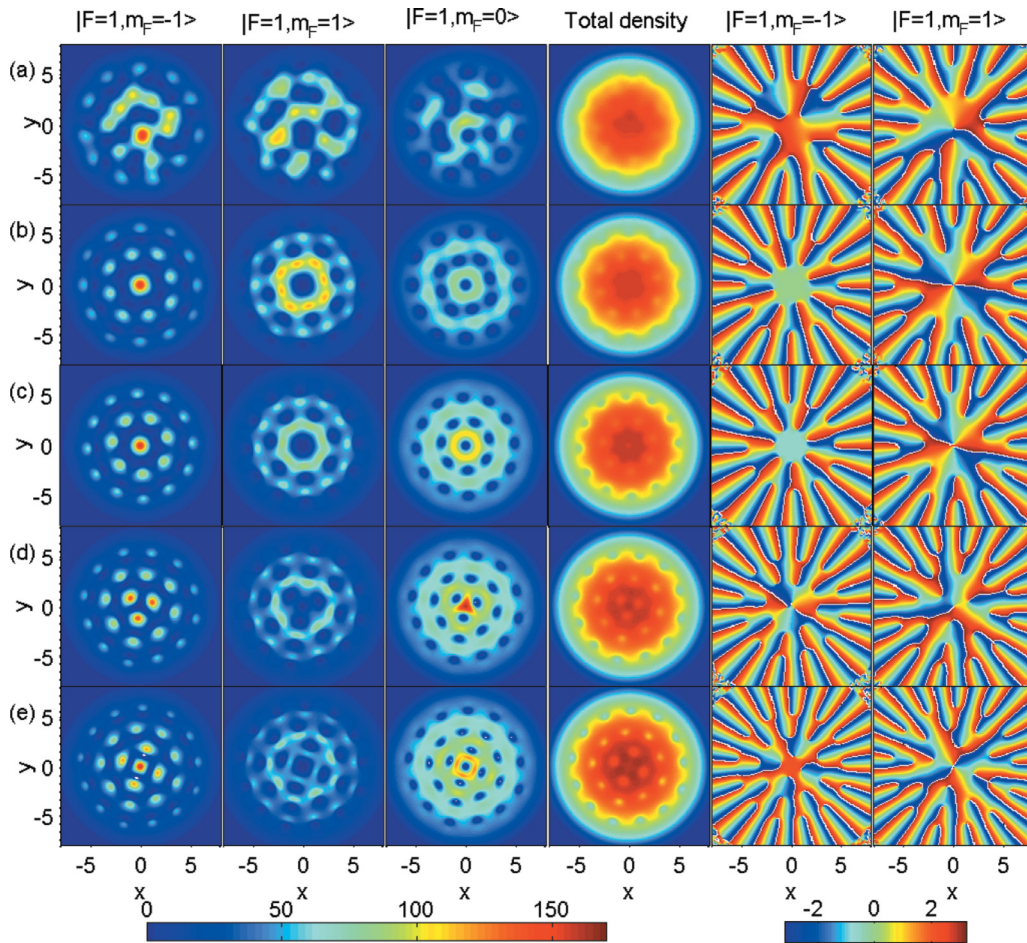$$s_{0y} = -\sqrt{1 - s_{0x}^2 - s_{0z}^2},$$

FIG. 3. (Color online) The densities and phases of the spinor BEC of ^{87}Rb with SOC κ when the system reaches the equilibrium state. (a) $\kappa = 0.1$; (b) $\kappa = 0.2$; (c) $\kappa = 0.5$; (d) $\kappa = 0.7$; (e) $\kappa = 1.0$. Here, $\Omega = 0.5\omega$, $a_0 = 101.8a_B$, and $a_2 = 100.4a_B$. Note that the fifth and sixth columns are the phases of the $m_F = -1$ and $m_F = 1$ components, respectively. The atom numbers (N_{-1}, N_1, N_0) approximately are $(5.1 \times 10^3, 5.5 \times 10^3, 5.7 \times 10^3)$, $(4.0 \times 10^3, 5.8 \times 10^3, 6.8 \times 10^3)$, $(4.0 \times 10^3, 5.5 \times 10^3, 8.1 \times 10^3)$, $(4.4 \times 10^3, 5.4 \times 10^3, 8.9 \times 10^3)$, and $(4.8 \times 10^3, 5.6 \times 10^3, 9.8 \times 10^3)$, respectively. The units of length and strength of SOC are $\sqrt{\hbar/(m\omega)}$ and $\sqrt{\hbar\omega/m}$, respectively.
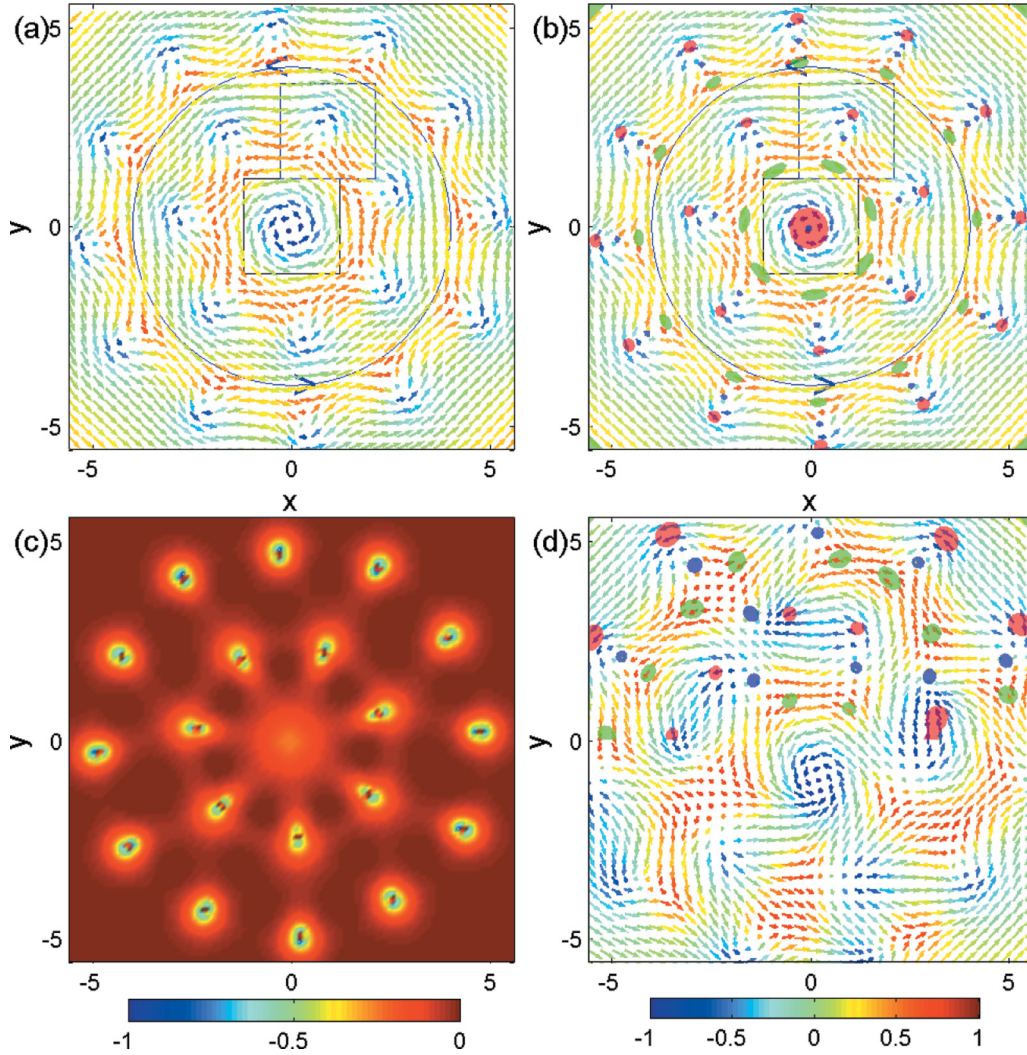
FIG. 4. (Color online) (a) Spin texture of spinor BEC of ^{87}Rb with $\kappa = 0.5$ and $\Omega = 0.5\omega$. The color of each arrow indicates the magnitude of S_z. The black pane points out a skyrmion, and the blue pane indicates a half-skyrmion. The blue arrows show the main direction of the spin texture. (b) The position of the vortices and the spin texture. The green, blue, and red spots are the center of vortices formed by the $m_F = -1$, $m_F = 0$, and $m_F = +1$ components, respectively. (c) Topological charge density. (d) The position of the vortices and the spin texture of spinor BEC of ^{87}Rb with $\kappa = 0.1$ and $\Omega = 0.5\omega$. Note that we only mark the vortices in the $y > 0$ region in order to illuminate the spin texture and the position of the vortices clearly. The units of length and strength of SOC are $\sqrt{\frac{\hbar}{m\omega}}$ and $\sqrt{\hbar\omega/m}$, respectively.

where λ is a variable parameter. Clearly, the two vectors $\mathbf{s}_{0x}$ and $\mathbf{s}_{0z}$ can vary from -1 to 1, but the vector $\mathbf{s}_{0y}$ varies from -1 to 0. This means that the spin vector can cover half of a unit sphere. By calculating the topological charge $Q = \frac{1}{4\pi} \iint \mathbf{s} \cdot (\frac{\partial \mathbf{S}}{\partial x} \times \frac{\partial \mathbf{S}}{\partial y}) dx dy$, where $\mathbf{s} = \mathbf{S}/|\mathbf{S}|$ and $\mathbf{S}$ comes from Eq. (3), we find the topological charge approaches $|Q| = 0.5$. Note that the value of the topological charge with Eqs. (4) is $|Q| = 0.5$. If we perform a transformation: $(\mathbf{S}'_x, \mathbf{S}'_y, \mathbf{S}'_z) = (\mathbf{S}_x, \mathbf{S}_z, \mathbf{S}_y)$, we can obtain a clear skyrmion-like structure [see Fig. 1(d)]. Meanwhile, we can prove that the transformation does not affect the value of the topological charge $|Q|$ at all. The explicit proofs are given in the Appendix. Thus, the spin texture in Fig. 1(c) is a half-skyrmion.

In Refs. [36,37], Kasamatsu *et al.* have studied the meron-antimeron pair in the two-component BECs without SOC. They have provided expressions to characterize the

meron-antimeron pair. In Ref. [38], Su *et al.* have also obtained the meron-antimeron pair by simulating the nonrotating spinor BEC of ^{87}Rb with SOC. Our study indicates that in the rotating BECs with SOC the half-skyrmion (meron) can appear without pairing. Meanwhile, the solution [Eqs. (4)] is completely different from that in Ref. [36]. We remark that the above transformation exchanges the spin vectors in Fig. 1(d). It mainly changes the perspective but does not affect the essence of the spin texture.

Figure 1(e) indicates the local density distribution in the region of the half-skyrmion. The green, blue, and red surfaces represent the densities of the $m_F = -1$, $m_F = 0$, and $m_F = +1$ components, respectively. The cyan represents the total density. The $m_F = +1$ component forms an obvious hump in the vortex region of the $m_F = -1$ component, and vice versa for the $m_F = -1$ component. These properties cause a dipole

of spin. There is a local density minimum at the position of the vortex formed by the $m_F = 0$ component when we examine the total density. This point is different from the normal coreless vortex [34–37,39,40] where the total density has no singularity. In fact, this structure can be viewed as a three-vortex structure. In the following text, we show that the three-vortex structure plays an important role in creating the half-skyrmion.

Figure 2 plots a half-skyrmion with Eqs. (4). Comparing it with Fig. 1(c), the formation of the two spin textures is very similar. This indicates the half-skyrmion can be well described by Eqs. (4) in our simulation. We obtain Eqs. (4) to characterize the half-skyrmion intuitively according to the properties of Fig. 1(c). All the arrows in Fig. 1(c) tend to point down, which means the spin vector $\mathbf{s}_{0y} \leqslant 0$. Especially the arrows completely point down when the position is far away from $(-2,0)$, this property means that $\mathbf{s}_{0x}$ and $\mathbf{s}_{0z}$ should approach 0 when the position is far away from the half-skyrmion. Thus, there must be an index function in the expression of the spin vectors $\mathbf{s}_{0x}$ and $\mathbf{s}_{0z}$, respectively. Furthermore, we have found that the half-skyrmion is related to a three-vortex structure, which causes a dipole of spin. This feature implies that $\mathbf{s}_{0x}$ and $\mathbf{s}_{0z}$ would be antisymmetrical. With lots of tests on the topological charge and others, we find Eqs. (4) can characterize the half-skyrmion. Note that there is a displacement of position between the two plots [Figs. 1(c) and 2].

B. Half-skyrmion lattice in rotating spin-1 BEC with spin-orbit coupling

To obtain the half-skyrmion lattice, we choose the following parameters: $\mu_{j,0}(j = 0, \pm 1) = 3.6\hbar\omega$, $\mu = 25\hbar\omega$, $\kappa_x = \kappa_y = \kappa$, and the rotating frequency $\Omega = 0.5\omega$. Figure 3 displays the densities and phases obtained under various strengths of SOC. For a very weak SOC ($\kappa = 0.1$), the patterns are irregular. When κ is over 0.1, the patterns are relatively regular. We take the $m_F = 1$ component as an example. In Fig. 3(b), there are eight nearest vortices around the center vortex of the $m_F = 1$ component. There are seven, three, and four in Figs. 3(c), 3(d), and 3(f), respectively. Thus, these pictures factually display the transition of the patterns as the strength of SOC increases. SOC can be used to adjust the pattern of the rotating spin-1 BEC.

Just as in previous experiments about the rotating BECs [30,31], there are some vortices in the three components respectively. The fifth and sixth columns indicate the phases of the $m_F = -1$ and $m_F = 1$ components, respectively. Like the vortex lattice in the single-component BEC, there are some lines where the phases change discontinuously from red to blue, which corresponds to the branch cuts between the phases $-\pi$ and π. The ends represent phase defects. All the lines extend to the outskirts of the BEC, where the density of the BEC is almost negligible, and end with another defect which offers neither the energy nor the angular momentum to the system. Furthermore, we also find some peaks accompanying the vortices, regularly arraying to be trianglar, square, heptagonal, etc., especially in the center of the $m_F = -1$ component.

Unlike the periodic vortex lattice [30] or the vortices trimers [31], the vortices encircle the center with several circles. The number of vortices is 1 or 0 in the center, and it increases as
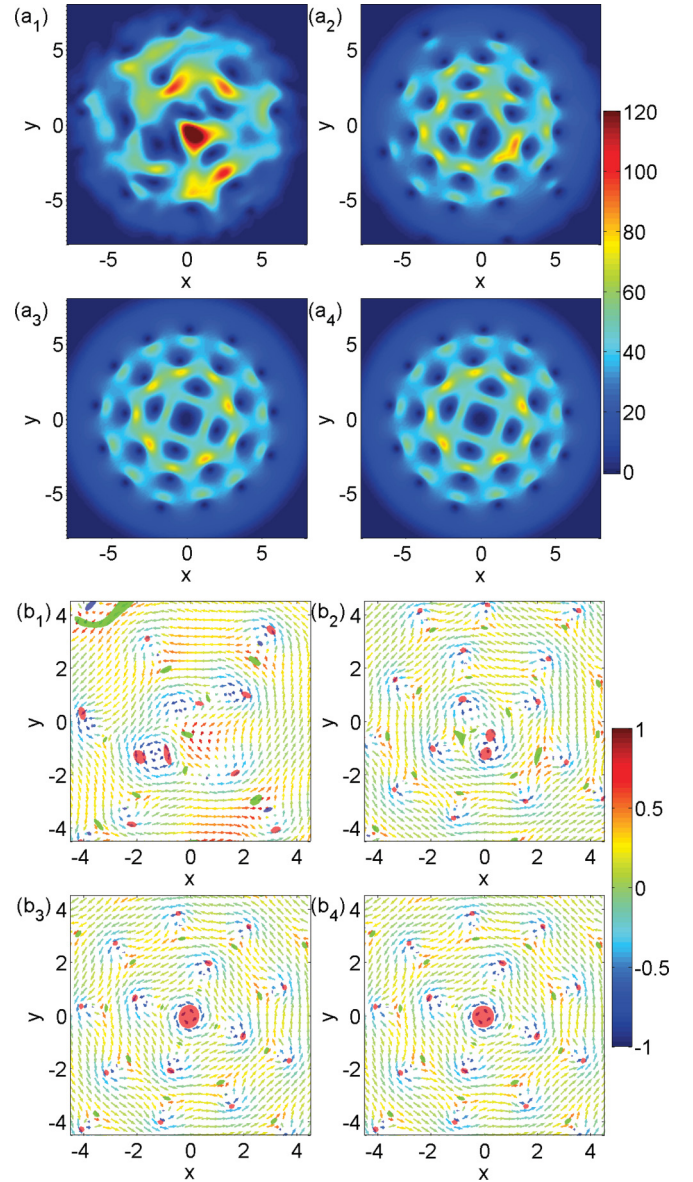

FIG. 5. (Color online) The time evolution of the spin-1 BEC of ^{87}Rb with $\mu_{j,0}(j = 0, \pm 1) = 3.6\hbar\omega$, $\mu = 25\hbar\omega$, $\kappa_x = \kappa_y = 1$, and $\Omega = 0.5\omega$. Panels (a$_1$)–(a$_4$) show the densities of the $m_F = 1$ component at $t = 20\omega^{-1}$, $60\omega^{-1}$, $200\omega^{-1}$, and $500\omega^{-1}$, respectively; panels (b$_1$)–(b$_4$) show the corresponding spin texture and the position of vortices. The meanings of the spots and the colored arrows are the same as those in Fig. 4(b). The units of length and strength of SOC are $\sqrt{\frac{\hbar}{m\omega}}$ and $\sqrt{\hbar\omega/m}$, respectively.

the radius increases. Certainly, this phenomenon is not obvious when SOC is very weak ($\kappa = 0.1$). The fourth column shows the total density of BECs. Here, we can distinguish some local minimum of densities, especially when κ approaches 1.

Two components of the BECs have a corresponding vortex at the center and the other component forms a hump filled in the center vortices. In addition, one of the center vortices is formed by the $m_F = 1$ component. For example, the $m_F = 0$ and $m_F = 1$ components have a corresponding center vortex in Figs. 3(b), 3(c), and 3(e). However, in Fig. 3(d), the center vortex is created in the $m_F = -1$ and $m_F = 1$
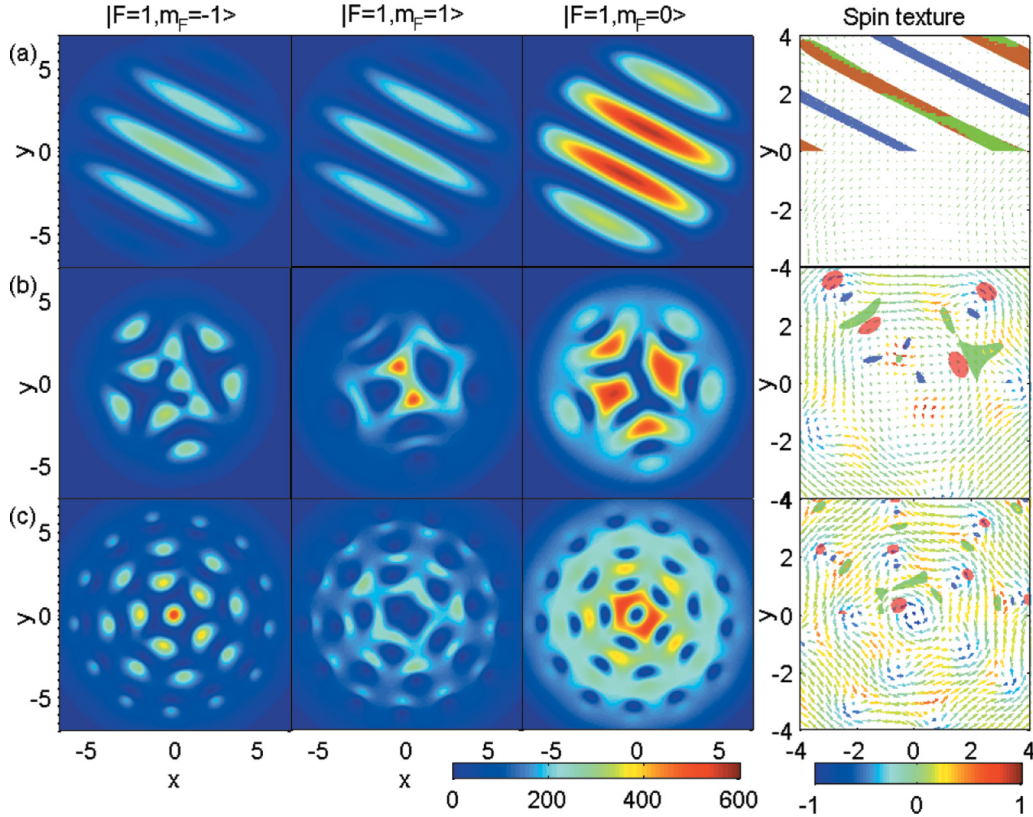
FIG. 6. (Color online) The effect of rotation frequency Ω for spinor BEC of ^{23}Na with $\mu_{j,0}(j = 0, \pm 1) = 3.6\hbar\omega$, $\mu = 25\hbar\omega$, $\kappa_x = \kappa_y = \kappa = 1$, $a_0 = 50a_B$, and $a_2 = 55a_B$. (a) $\Omega = 0$; (b) $\Omega = 0.2\omega$; (c) $\Omega = 0.5\omega$. The fourth column shows the corresponding spin textures and the positions of the vortices. The meanings of the spots and the colored arrows are the same as those in Fig. 4(b). Note that we only mark the vortices in the $y > 0$ region. The atom numbers (N_{-1}, N_1, N_0) approximately are $(1.2 \times 10^4, 1.2 \times 10^4, 2.36 \times 10^4)$, $(1.13 \times 10^4, 1.5 \times 10^4, 2.46 \times 10^4)$, and $(1.67 \times 10^4, 2.0 \times 10^4, 3.53 \times 10^4)$, respectively. The units of length and strength of SOC are $\sqrt{\frac{\hbar}{m\omega}}$ and $\sqrt{\hbar\omega/m}$, respectively.

components, respectively. A center vortex is formed in which two components depend on lots of factors such as the number of vortices, the number of atoms of each component, the rotation frequency and the strength of SOC. Generally, if the center vortex of the $m_F = 1$ component is a multiply charged vortex, the other center vortex will occur in the $m_F = 0$ component. Otherwise, the other center vortex will occur in the $m_F = -1$ component.

There are many half-skyrmions rounding the center several circles, i.e., radially arranging in the system [see Fig. 4(a)]. Meanwhile, the arrows form big rings, whose main direction is marked with the blue arrows. Figure 4(b) illuminates the relationship between the vortices and the half-skyrmions. Except for the central area of the BECs, we find the positions of vortices in the three components are far away from the center with the following order: green, blue, and red. Meanwhile, the sequence distributes in the whole system. Furthermore, Figure 4(c) plots the topological charge density, which is defined by $q(r) = \frac{1}{4\pi}\mathbf{s} \cdot (\frac{\partial \mathbf{S}}{\partial x} \times \frac{\partial \mathbf{S}}{\partial y})$, where $\mathbf{s} = \mathbf{S}/|\mathbf{S}|$. The value of the topological charge density varies only from -1 to 0. This property indicates that our results in Fig. 4(a) are half-skyrmions but not meron-antimeron pairs. Obviously, each half-skyrmion with the nontrivial topological charge density accompanies a three-vortex structure. Thus, we can view the three-vortex structure as a cell. Undoubtedly, the

number of vortices in three components approaches $1:1:1$. Usually, the skyrmion-like excitations [34–37] are related to the underlying vortex configuration such as Mermin-Ho [39] and Anderson-Toulouse [40] vortices. Here, the half-skyrmion is related to the three-vortex structure. The distribution of half-skyrmions depends on that of vortices. Thus, it is not inconceivable that the different strengths of SOC will cause various half-skyrmion lattices.

In the absence of SOC, the periodic skyrmion lattice can be created in the rotating spin-1 BEC of ^{87}Rb [31]. Figure 4(d) shows the spin textures and the positions of vortices when the strength of SOC is 0.1. The vortices hardly form the three-vortex structure, especially near the center. Additionally, the half-skyrmion lattice is not very obvious. These results further prove that the half-skyrmion is related to the three-vortex structure. To obtain the half-skyrmion lattice, the strength of SOC must exceed a critical value. Here, this value approaches 0.2. Note that we do not fix the ratio of the three components in the dynamical process. The mixture ratio of the three components depends on the system itself.

Figure 5 indicates the time evolution of the system. Here, we take ^{87}Rb with $\mu_{j,0}(j = 0, \pm 1) = 3.6\hbar\omega$, $\mu = 25\hbar\omega$, $\kappa_x = \kappa_y = 1$, and $\Omega = 0.5\omega$ as an example. Figures 5(a$_1$)– 5(a$_4$) indicate the densities of the $m_F = 1$ component at
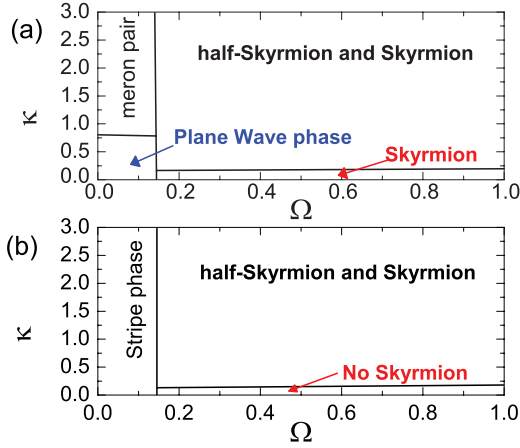
FIG. 7. (Color online) The phase diagrams of the products in spin-1 BEC with the rotation frequency Ω and the SOC strength κ ($\kappa_x = \kappa_y = \kappa$). Here, $\mu_{j,0}(j = 0, \pm 1) = 3.6\hbar\omega$ and $\mu = 25\hbar\omega$. (a) ^{87}Rb. (b) ^{23}Na. The units of rotation frequency and strength of SOC are ω and $\sqrt{\hbar\omega/m}$, respectively.

$t = 20\omega^{-1}, 60\omega^{-1}, 200\omega^{-1}$, and $500\omega^{-1}$, respectively. The density distributions in Figs. 5(a_1), 5(a_2), and 5(a_3) are different from each other. However, the density distribution in Fig. 5(a_3) is almost the same as that in Fig. 5(a_4). These properties mean that the system has reached the equilibrium state and the density distribution is dynamically stable. Similarly, the $m_F = -1$ and $m_F = 0$ components also have these properties.
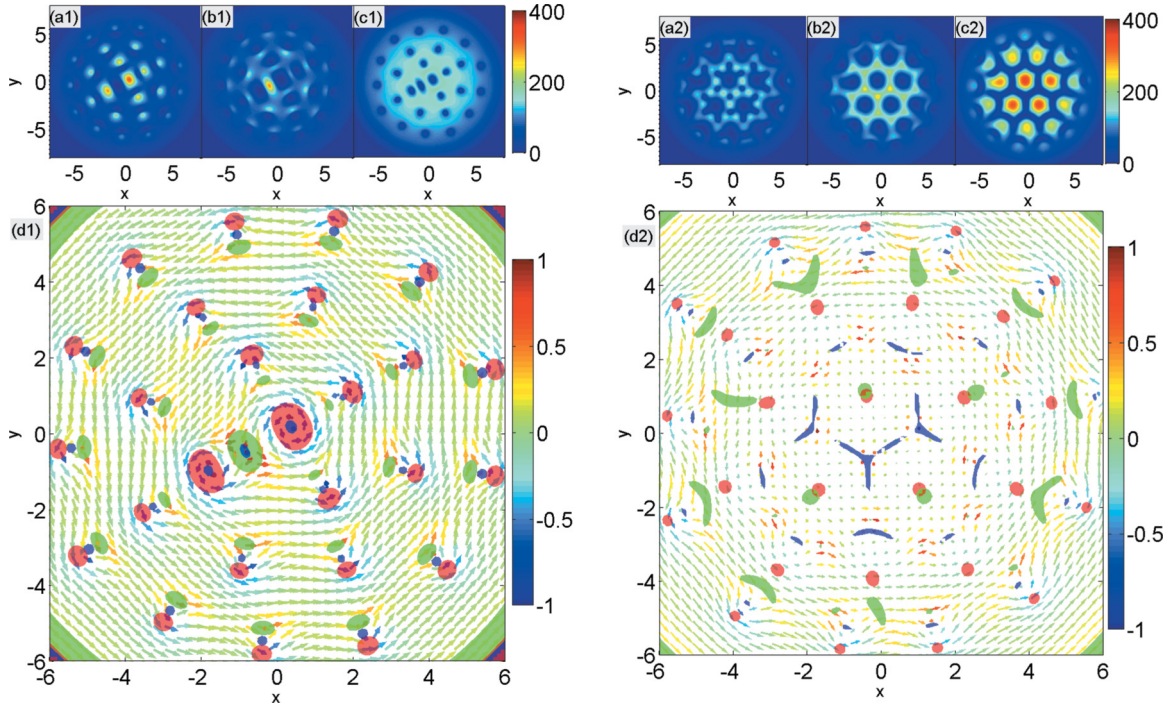
Figures 5(b_1)–5(b_4) are the corresponding spin textures at $t = 20\omega^{-1}, 60\omega^{-1}, 200\omega^{-1}$, and $500\omega^{-1}$, respectively. Obviously, the spin texture is stable when the system reaches the equilibrium state. In fact, all the results are dynamically stable when the system reaches the equilibrium state under the quenching process.

C. The effect of the rotation frequency

We find the half-skyrmion lattice can also occur in the antiferromagnetic (AFM) BEC, where $g_s > 0$ [see Fig. 6(c)]. There is no skyrmion excitation appearing in the rotating AFM BEC of ^{23}Na [31] when $\kappa = 0$. Here, we use the spinor BEC of ^{23}Na to illustrate the effect of the rotation frequency. We only change the rotation frequency Ω and fix all other parameters to perform the numerical experiments. Figure 6 shows the density distribution and spin texture under various rotation frequencies. In the absence of rotation ($\Omega = 0$), there is no vortex appearing at all. Each component of the BECs is split into several parallel parts. In fact, these properties agree with the stripe phase [19–22]. The spin texture indicates no half-skyrmion excitations in this system. Color straps factually are the low density domain of BECs. With the addition of a weak rotation (0.2ω), the splitting parts bend and break, and several vortices and the three-vortex structure occur. When the rotation becomes faster (0.5ω), the vortex lattice emerges and the half-skyrmion lattice is very obvious. Naturally, the rotation can

FIG. 8. (Color online) The effect of tuning FM and AFM interactions for BEC with $\mu_{j,0}(j = 0, \pm 1) = 3.6\hbar\omega$, $\mu = 25\hbar\omega$, $\kappa_x = \kappa_y = 1$, and $\Omega = 0.5\omega$. Panels (a1), (b1), and (c1) show the densities of the $m_F = -1$, $m_F = 1$, and $m_F = 0$ components of ^{87}Rb with $a_0 = 101.8a_B$ and $a_2 = 50.2a_B$, respectively ($N_{-1} \approx 1.0 \times 10^4$, $N_1 \approx 1.1 \times 10^4$, $N_0 \approx 1.91 \times 10^4$) (strong FM case). Panel (d1) shows the spin texture and the positions of the vortices. The meanings of the spots and the colored arrows are the same as those in Fig. 4(b). Panels (a2)–(d2) indicate the corresponding results of ^{23}Na with $a_0 = 50a_B$ and $a_2 = 110a_B$ ($N_{-1} \approx 9.2 \times 10^3$, $N_1 \approx 1.2 \times 10^4$, $N_0 \approx 1.75 \times 10^4$) (strong AFM case). The units of length and strength of SOC are $\sqrt{\frac{\hbar}{m\omega}}$ and $\sqrt{\hbar\omega/m}$, respectively.

control the half-skyrmion lattice because it can induce the underlying vortices.

Now, we can systematically understand the half-skyrmion phenomenon in the rotating spinor BECs. Its dynamics is driven by the rotation in the quenching process and the intrinsic spin-Hall effect derived from the effective SOC. As is well known in the study of rotating superfluid helium [41,42], the rotating drive pulls vortices into the rotation axis, while repulsive interaction tends to push them apart; this competition yields a vortex lattice whose vortex density depends on the rotation frequency. Meanwhile, SOC causes the spin separation and creates the dipole structure of spin, which is embedded in the three-vortex structure. The half-skyrmion derives from the dipole structure. In terms of densities, only a core structure appears in the center. That is the origin of the center skyrmion.

Figure 7 plots the phase diagrams of the spinor BECs with various products in our experiments. In this paper, we mainly focus on the half-skyrmion as well as the center skyrmion. The half-skyrmion phase, where the center skyrmion may appear, occupies a large region of the Ω-κ plane in both the FM BEC and the AFM BEC. For the FM BEC of ^{87}Rb, the meron-antimeron pairs [38] can occur when SOC is greater than a critical value (≈ 0.8) and the rotation is very weak. Figure 7(a) also shows the condition for obtaining the plane wave phase ($\kappa \leqslant 0.8$, $\Omega \leqslant 0.15\omega$) and for creating the skyrmion lattice ($\kappa \leqslant 0.2$, $\Omega > 0.15\omega$). For the AFM BEC of ^{23}Na, the skyrmion or half-skyrmion hardly occurs when κ is smaller than 0.2 [see Fig. 7(b)]. If the rotation is very weak ($\Omega \leqslant 0.15\omega$), the stripe phase is observed.

D. The effect of tuning the FM and AFM interactions

Generally speaking, g_s is much smaller than g_n. By adjusting the two s-wave scattering lengths a_0 and a_2 through Feshbach resonances, the spin exchange interaction strength g_s is tunable. We now perform the above experiments by changing a_2. Figures 8(a1)–(d1) show a stronger FM case of ^{87}Rb ($g_s/g_n = -0.255$). Contrasting the densities and the spin texture, we find the three-vortex structure and the half-skyrmion lattice are common in this FM BEC, though there are several half-skyrmions of the circular/hyperbolic structure near the center. Furthermore, we also test a stronger AFM BEC of ^{23}Na ($g_s/g_n = 0.222$). The three-vortex structure and the half-skyrmion mainly emerge at the outskirts of the BECs. In fact, the strong AFM interactions restrict the half-skyrmion excitations, so the half-skyrmion hardly emerges in the center. If we increase the strength of SOC, we will obtain a more obvious picture about the half-skyrmion lattice. These experiments show the universality of the half-skyrmion excitation in BECs with SOC.

IV. CONCLUSION

We have studied the half-skyrmion in the rotating spin-1 BEC with SOC. We find the half-skyrmions (meron) can occur but do not form the meron-antimeron pairs. This phenomenon implies a new understanding of the half-skyrmion in BECs. The half-skyrmion originates from a dipole that resulted from a local spin separation. Meanwhile, the half-skyrmion excitation

is related to a three-vortex structure where the dipole is embedded. The half-skyrmion excitation can occur as long as the three-vortex structure appears, even in the strong FM and AFM BECs with SOC. The provided phase diagrams indicate the condition of obtaining the half-skyrmions in spinor BECs of both ^{87}Rb and ^{23}Na. Our study gives an experimental protocol to observe these phenomena in future experiments. Not only do our findings exist in spin-1 BEC, but also the related textures should appear in high-spin BEC, superfluid, and superconduction. This work is of particular significance for exploring the topological excitations such as half-skyrmions in quantum gas and condensed matter physics.

APPENDIX: THE NUMERICAL PROOFS ON THE UNCHANGED TOPOLOGICAL CHARGE $|Q|$ UNDER THE TRANSFORMATION $(\mathbf{S}'_x, \mathbf{S}'_y, \mathbf{S}'_z) = (\mathbf{S}_x, \mathbf{S}_z, \mathbf{S}_y)$

We now prove that the topological charge $|Q|$ is unchanged under the transformation $(\mathbf{S}'_x, \mathbf{S}'_y, \mathbf{S}'_z) = (\mathbf{S}_x, \mathbf{S}_z, \mathbf{S}_y)$. It is well known that the topological charge Q is defined as

$$Q = \frac{1}{4\pi} \iint \mathbf{s} \cdot \left(\frac{\partial \mathbf{s}}{\partial x} \times \frac{\partial \mathbf{s}}{\partial y} \right) dx\,dy, \tag{A1}$$

where $\mathbf{s} = \mathbf{S}/|\mathbf{S}|$. For clarity, we use $Q(\mathbf{s}_x, \mathbf{s}_y, \mathbf{s}_z)$ to describe the normal expression of the topological charge Q of Eq. (A1) and $Q(\mathbf{s}_x, \mathbf{s}_z, \mathbf{s}_y)$ to denote the topological charge under the transformation $(\mathbf{S}'_x, \mathbf{S}'_y, \mathbf{S}'_z) = (\mathbf{S}_x, \mathbf{S}_z, \mathbf{S}_y)$.

We can expand the expression $Q(\mathbf{s}_x, \mathbf{s}_y, \mathbf{s}_z)$ to be

$$Q(\mathbf{s}_x, \mathbf{s}_y, \mathbf{s}_z) = \frac{1}{4\pi} \iint \begin{vmatrix} \mathbf{s}_x & \mathbf{s}_y & \mathbf{s}_z \\ \frac{\partial}{\partial x}\mathbf{s}_x & \frac{\partial}{\partial x}\mathbf{s}_y & \frac{\partial}{\partial x}\mathbf{s}_z \\ \frac{\partial}{\partial y}\mathbf{s}_x & \frac{\partial}{\partial y}\mathbf{s}_y & \frac{\partial}{\partial y}\mathbf{s}_z \end{vmatrix} dx\,dy.$$

Similarly, $Q(\mathbf{s}_x, \mathbf{s}_z, \mathbf{s}_y)$ can be written as

$$Q(\mathbf{s}_x, \mathbf{s}_z, \mathbf{s}_y) = \frac{1}{4\pi} \iint \begin{vmatrix} \mathbf{s}_x & \mathbf{s}_z & \mathbf{s}_y \\ \frac{\partial}{\partial x}\mathbf{s}_x & \frac{\partial}{\partial x}\mathbf{s}_z & \frac{\partial}{\partial x}\mathbf{s}_y \\ \frac{\partial}{\partial y}\mathbf{s}_x & \frac{\partial}{\partial y}\mathbf{s}_z & \frac{\partial}{\partial y}\mathbf{s}_y \end{vmatrix} dx\,dy$$

$$= -\frac{1}{4\pi} \iint \begin{vmatrix} \mathbf{s}_x & \mathbf{s}_y & \mathbf{s}_z \\ \frac{\partial}{\partial x}\mathbf{s}_x & \frac{\partial}{\partial x}\mathbf{s}_y & \frac{\partial}{\partial x}\mathbf{s}_z \\ \frac{\partial}{\partial y}\mathbf{s}_x & \frac{\partial}{\partial y}\mathbf{s}_y & \frac{\partial}{\partial y}\mathbf{s}_z \end{vmatrix} dx\,dy$$

$$= -Q(\mathbf{s}_x, \mathbf{s}_y, \mathbf{s}_z).$$

Thus, we obtain $Q(\mathbf{s}_x, \mathbf{s}_y, \mathbf{s}_z) = -Q(\mathbf{s}_x, \mathbf{s}_z, \mathbf{s}_y)$ and $|Q(\mathbf{s}_x, \mathbf{s}_y, \mathbf{s}_z)| = |Q(\mathbf{s}_x, \mathbf{s}_z, \mathbf{s}_y)|$. The topological charge $|Q|$ is unchanged under the transformation $(\mathbf{S}'_x, \mathbf{S}'_y, \mathbf{S}'_z) = (\mathbf{S}_x, \mathbf{S}_z, \mathbf{S}_y)$.

Similarly, the topological charge $|Q|$ is unchanged, no matter how we exchange the spin vectors $\mathbf{S}_x$, $\mathbf{S}_y$, and $\mathbf{S}_z$.

[1] Y. A. Bychkov and E. I. Rashba, J. Phys. C **17**, 6039 (1984).
[2] G. Dresselhaus, Phys. Rev. **100**, 580 (1955).
[3] A. M. Dudarev, R. B. Diener, I. Carusotto, and Q. Niu, Phys. Rev. Lett. **92**, 153005 (2004).
[4] Y. K. Kato, R. C. Myers, A. C. Gossard, and D. D. Awschalom, Science **306**, 1910 (2004).
[5] M. König, S. Wiedmann, C. Brüne, A. Roth, H. Buhmann, L. W. Molenkamp, X.-L. Qi, and S.-C. Zhang, Science **318**, 766 (2007).
[6] C. L. Kane and E. J. Mele, Phys. Rev. Lett. **95**, 146802 (2005).
[7] B. A. Bernevig, T. L. Hughes, and S.-C. Zhang, Science **314**, 1757 (2006).
[8] D. Hsieh, D. Qian, L. Wray, Y. Xia, Y. S. Hor, R. J. Cava, and M. Z. Hasan, Nature (London) **452**, 970 (2008).
[9] K. Sun, W. V. Liu, A. Hemmerich, and S. D. Sarma, Nat. Phys. **8**, 67 (2012).
[10] Y.-J. Lin, K. Jiménez-García, and I. B. Spielman, Nature (London) **471**, 83 (2011).
[11] R. Liao, Y. Yi-Xiang, and W.-M. Liu, Phys. Rev. Lett. **108**, 080406 (2012).
[12] J. Ruseckas, G. Juzeliunas, P. Öhberg, and M. Fleischhauer, Phys. Rev. Lett. **95**, 010404 (2005).
[13] K. Osterloh, M. Baig, L. Santos, P. Zoller, and M. Lewenstein, Phys. Rev. Lett. **95**, 010403 (2005).
[14] I. I. Satija, D. C. Dakin, and C. W. Clark, Phys. Rev. Lett. **97**, 216401 (2006).
[15] S. L. Zhu, H. Fu, C. J. Wu, S. C. Zhang, and L. M. Duan, Phys. Rev. Lett. **97**, 240401 (2006).
[16] X. J. Liu, X. Liu, L. C. Kwek, and C. H. Oh, Phys. Rev. Lett. **98**, 026602 (2007).
[17] T. D. Stanescu, C. Zhang, and V. Galitski, Phys. Rev. Lett. **99**, 110403 (2007).
[18] G. Juzeliunas, J. Ruseckas, and J. Dalibard, Phys. Rev. A **81**, 053403 (2010).
[19] C. Wang, C. Gao, C.-M. Jian, and H. Zhai, Phys. Rev. Lett. **105**, 160403 (2010).
[20] T.-L. Ho and S. Z. Zhang, Phys. Rev. Lett. **107**, 150403 (2011).
[21] C.-M. Jian and H. Zhai, Phys. Rev. B **84**, 060508(R) (2011).
[22] S. Sinha, R. Nath, and L. Santos, Phys. Rev. Lett. **107**, 270401 (2011).
[23] H. Hu, B. Ramachandhran, H. Pu, and X.-J. Liu, Phys. Rev. Lett. **108**, 010402 (2012).
[24] C. Wu, I. Mondragon-Shem, and X. F. Zhou, Chin. Phys. Lett. **28**, 097102 (2011).
[25] X.-Q. Xu and J. H. Han, Phys. Rev. Lett. **107**, 200401 (2011).
[26] X.-F. Zhou, J. Zhou, and C. Wu, Phys. Rev. A **84**, 063624 (2011).
[27] V. Schweikhard, I. Coddington, P. Engels, S. Tung, and E. A. Cornell, Phys. Rev. Lett. **93**, 210403 (2004).
[28] T. Mizushima, N. Kobayashi, and K. Machida, Phys. Rev. A **70**, 043613 (2004).
[29] J.-P. Martikainen, A. Collin, and K.-A. Suominen, Phys. Rev. A **66**, 053604 (2002).
[30] A. S. Bradley, C. W. Gardiner, and M. J. Davis, Phys. Rev. A **77**, 033616 (2008).
[31] S.-W. Su, C.-H. Hsueh, I.-K. Liu, T.-L. Horng, Y.-C. Tsai, S.-C. Gou, and W. M. Liu, Phys. Rev. A **84**, 023601 (2011).
[32] S. J. Rooney, A. S. Bradley, and P. B. Blakie, Phys. Rev. A **81**, 023630 (2010).
[33] F. Zhou, Phys. Rev. Lett. **87**, 080401 (2001).
[34] T. Mizushima, K. Machida, and T. Kita, Phys. Rev. Lett. **89**, 030401 (2002).
[35] T. Mizushima, N. Kobayashi, and K. Machida, Phys. Rev. A **70**, 043613 (2004).
[36] K. Kasamatsu, M. Tsubota, and M. Ueda, Phys. Rev. Lett. **93**, 250406 (2004).
[37] K. Kasamatsu, M. Tsubota, and M. Ueda, Phys. Rev. A **71**, 043611 (2005).
[38] S.-W. Su, I.-K. Liu, Y.-C. Tsai, W. M. Liu, and S.-C. Gou, Phys. Rev. A **86**, 023601 (2012).
[39] N. D. Mermin and T.-L. Ho, Phys. Rev. Lett. **36**, 594 (1976).
[40] P. W. Anderson and G. Toulouse, Phys. Rev. Lett. **38**, 508 (1977).
[41] L. J. Campbell and R. M. Ziff, Phys. Rev. B **20**, 1886 (1979).
[42] M. Tsubota and H. Yoneda, J. Low Temp. Phys. **101**, 815 (1995).